Sustainability in Environment
ISSN 2470-637X (Print) ISSN 2470-6388 (Online)
Vol. 11, No. 1, 2026
www.scholink.org/ojs/index.php/se

Original Paper

Meteorological Drivers of Summertime Ground-Level Ozone in Jilin City (2020-2023): WRF–CMAQ Simulation and Health Risk Assessment

Anees Akhtar[1], Chunsheng Fang[1*], Muhammad Yousuf Jat Baloch[2], & Ju Wang[1]

[1] College of New Energy and Environment, Jilin University, Changchun 130012, China

[2] School of Environmental Science and Engineering, Shandong University, Qingdao, Shandong, China

[*] Corresponding Author: Chunsheng Fang (fangcs@jlu.edu.cn)

Received: December 23, 2025 Accepted: February 06, 2026 Online Published: February 25, 2026

doi:10.22158/se.v11n1p186 URL: http://dx.doi.org/10.22158/se.v11n1p186

Abstract

The rising incidence of ground-level ozone (O_3) air pollution and its subsequent adverse health effects in urban areas, particularly in emerging countries such as China, warrant urgent attention. Ground-level O_3 is a major health threat, accelerating respiratory diseases and cardiovascular disorders. Despite widespread studies in major industrial areas, the spatial and temporal patterns of O_3 are, however, insufficient, particularly for smaller cities such as Jilin, North China, with reference to meteorological forcing. The study aims to bridge this gap through an analysis of the spatiotemporal variability of O_3 and related health effects for the period 2020 to 2023 for the summer seasons (May to July) for Jilin City, incorporating both meteorological and air quality models (WRF v4.3.3 and CMAQ v5.4) with inputs from various monitoring stations. The findings reveal that the higher temperatures in 2023 facilitated the production of O_3, whereas changes in the wind pattern and lower planetary boundary layer height influenced the transport of pollutants. The seasonal variations of O_3 were, however, underpredicted for the peak occurrences using the CMAQ model, with a normalised mean bias ranging from −30.98% to −22.98%. The health risk for the period, as indicated by the Normalised Health-based Air Quality Index (NHAQI), showed an improvement, albeit slight, in air quality from 2020 to 2023, accompanied by a decrease in the excess health risk (from 2.19% to 2.13%). The spatial analysis revealed continuous areas of high risk, particularly during stagnation periods in urban areas. The study highlights the importance of localized, season-oriented strategies for mitigating O_3 exposure and minimizing harm to public health. However, the marginal air quality improvement for the period 2020–2023 is encouraging, suggesting further improvement is possible. Increased accuracy must be

achieved through model improvements, refined emission inventories, and targeted remedies at locations with excessive O_3 levels, particularly sensitive urban locations.

Keywords

Ground-level ozone, meteorological factors, WRF-CMAQ model, air pollution, health risk assessment

1. Introduction

Ground-level ozone (O_3) is among the major secondary air pollutants that are generated within the troposphere due to the photochemical interaction between volatile organic compounds (VOCs) and nitrogen oxides (NOx) in the presence of sunlight (Touhami et al., 2024). Unlike the direct release of primary air pollutants to the atmosphere, a chain of atmospheric chemistry processes results in the production of O_3. The process is initiated with the photolysis process of the constituents of nitrogen dioxide (NO_2) under sunlight, with the presence of VOCs as co-reactants (P. Wang et al. 2022). The precursor pool is constructed through anthropogenic sources, including industrial activities, transportation, and the combustion of fossil fuels, as well as natural sources, such as biogenic emissions resulting from the presence of vegetation. The vegetation is responsible for the emission production of about 90% of total VOCs, and isoprene is the major biogenic emitter for VOCs (Ashworth, Wild, & Hewitt 2013). The non-linear atmospheric conditions and chemical regimes governing O_3 formation are either VOC-limited, NO_x-limited, or aerosol-inhibited regimes, whereby the formation of O_3 proceeds via the uptake of hydroperoxyl radicals (HO_2) by aerosol particles (Ivatt, Evans, and Lewis 2022). High O_3 concentrations are relatively favorable in urban and semi-urban environments, particularly during the summer. Elevated temperatures and high solar radiation lead to faster photochemical reactions, whereas a stagnant atmospheric environment allows pollutants to accumulate (Guo et al., 2024; Petrus, Popa, & Bratu 2024). Such factors are more dominant in most highly industrialized cities, such as Beijing, where large amounts of NOx and VOC gases have created a continuous state of high O_3 levels during summer periods (Zhao et al., 2018). There is good documentation on the health effects of O_3 exposure. Respiratory effects of acute exposure are respiratory tract irritation, cough, and throat irritation, and acute worsening of asthma, and chronic exposure has been linked with long-term respiratory illness, cardiovascular morbidity, and mortality risk development (Bell, Peng, & Dominici 2006; Jerrett et al., 2009; Trainer et al., 1993; Zhang et al., 2016). Children, elders, and individuals with existing diseases of the respiratory tract are the most exposed groups who are so impacted. Apart from the health of human individuals, O_3 is harmful to vegetation and affects agricultural production as well as environmental stability in peri-urban zones where the natural or agricultural environment overlaps with urban sprawl (Yin, Cao, & Wang, 2019).

The formation, transport, and accumulation of O_3 revolve around meteorological conditions. High temperatures increase reaction rates and also have a positive effect on emissions of some biogenic VOCs. The solar radiation is vital as it photolyzes NO_2 to create a chain of O_3 production (Ghazali et al., 2010; Jiang et al., 2021). Wind direction affects spatial O_3 distributions: strong winds will dilute

pollutants, lessening the concentration, whereas wind direction can transport O_3 and its precursors to the downwind region, potentially hundreds of kilometers away (Bai et al., 2021; Petrus et al., 2024). The environment is likely to promote O_3 accumulation with low humidity, for water vapor is an important radical sink for O_3 chemistry. Moreover, low levels of humidity are likely to promote the confinement of pollutants within shallow mixing layers at the surface, thus amplifying regional O_3 concentrations (Chen et al., 2022). Considering the character of these relations, weather variability exerts powerful effects on O_3 pollution patterns, requiring the application of meteorological parameters to air quality management policy making (Qiu et al. 2025; Yang et al. 2019). The case is representative of O_3 pollution studies, taking the city climate, localized meteorological environments, and emission sources under consideration. The emission sources point to coal combustion, featuring approximately 62% for the whole city, with the engine exhaust likely to account for approximately 19% (Bai et al., 2021). The prevailing wintertime pollutant is particulate matter derived from heating, whereas photochemically produced O_3 is predominant during the monsoon period. The surrounding environment of this place is similar to that around the Yangtze River Delta, whereby meteorological variables greatly modulate the extent of O_3 (Zhao et al., 2021). Anthropogenic and biogenic emissions are modulated by the regional meteorology at both anthropogenic and natural emission sources at the locations, resulting in O_3 occurrences. This indicates the importance of conducting location-specific studies to analyze regional air quality flow (Wang et al., 2022).

Summer 2023 is particularly ideal for this kind of research, having been a witness to a sequence of extreme weather events that generated exceedingly favorable circumstances for the production of O_3. Weeks with warm temperatures, gentle winds, and high air stability were seen—variables that are known to promote O_3 formation through the facilitation of biogenic emissions of VOCs and the acceleration of photochemical reactions (Zhang et al., 2018). Moderate to severe incidents, and, particularly, the periphery effects of typhoons, also yielded regional O_3 exceedances under specific instances through the increasing precursor availability. Similar instances were observed elsewhere, for instance, in the Pearl River Delta, where heatwaves were augmented through the effects of atmospheric inversions to significantly heighten air quality degradation. The increasingly frequent occurrence of extreme weather events through climate change serves to increase the need to examine the effects it exerts on O_3 air pollution (Yang & Shao, 2021).

Accurate evaluation of the health impacts of O_3 air pollution necessitates utilizing strong measurement approaches. Classic indices, such as the Air Quality Index (AQI), commonly do not adequately depict the associated health hazard for individual pollutants due to the fact that they aggregate numerous pollutants through a combined composite indicator, mainly emphasizing particulate matter (Cromar et al., 2020; Zhong, Yu, & Zhu, 2019). Health-oriented indices, such as the Health Air Quality Index (HAQI) and the Aggregate Air Quality Index (AAQI), exploit pollutant-specific exposure–response relations. The resulting evaluation is a more accurate and nuanced quantification of health hazards for both the short and long duration intervals (Motesaddi, Hashempour, & Nowrouz, 2017; Stieb et al.,

2005). These indices are also relevant for periods with peak O_3 concentrations, for the reason that they help with enhanced public reporting and support for timely reduction strategies. Despite widespread examination for terrestrial O_3 air pollution for highly urbanized and industrialized areas such as Beijing–Tianjin–Hebei (BTH), the Yangtze River Delta (YRD), and the Pearl River Delta (PRD), an immense knowledge gap is present for the clarification of O_3 dynamics in Northeast China, specifically for Jilin City. Previous studies were mostly carried out for areas with strong precursor emissions and monsoonal climatology, and consequently, the region of Northeast China is not adequately studied with respect to the meteorology at the local scale, synoptic weather patterns, and how these affect the formation of O_3 (Gao et al., 2020; Hu et al., 2024). The gap thus points to the need for location-specific studies that combine analyses of meteorological variability and health hazard appraisals to clarify O_3 air pollution mechanisms holistically for the region.

Accordingly, this study aimed to examine the spatiotemporal distribution of ground-level O_3 in Jilin City during the summers of 2020 and 2023, to explore the effects of meteorological variables on O_3 formation, and to quantify the associated health risk using sophisticated air quality models and newly proposed health indices. The investigation also aimed to develop future scenarios to determine how shifting weather patterns can affect O_3 air pollution and its associated health effects. It was assumed that meteorological variability in the summer of 2023, characterized by higher temperatures, weak winds, and stability, played a significant role in enhancing O_3 formation and health risks in Jilin City compared with the previous summer of 2020. In addition, the study assumed that coupling meteorological datasets with health risk indices can yield a more refined, localized evaluation of O_3 air pollution effects. The results of this study bridge a pertinent knowledge gap by documenting the comprehensive distribution of the impact that meteorological variability imposes on O_3 air pollution in the North China Plain. They support the formulation of effective, regionally specified mitigation strategies that promote public health and air quality planning for governance. The results also highlight the need for localized studies to address the problems associated with O_3 air pollution in the understudied urban region.

2. Methodology

2.1 Overview of the Study Area

Jilin City, also known as Beiguo River City, is a prefecture-level city in Jilin Province, northeastern China, with a total size of 17,200 square kilometers. It has been one of the largest industrial centers, serving as a central hub for industrial rebranding in the region, transforming the traditional industrial base. It is located between 42°31'N and 44°40'N, and 125°40'E and 127°56'E. At the end of 2021, the city of Jilin's registered population was around 4.018 million. It has four districts—Changyi, Chuanying, Fengman, and Longtan—and five county-level cities: Shulan, Panshi, Jiaohe, Huadian, and Yongji. It lies to the north of Harbin, east of Yanbian, west of Changchun and Siping, and south of Baishan, Tonghua, and Liaoyuan. Its terrain rises to the southeast, slopes northwest, and has mountains

to the side and rivers on three sides, making springs and autumns dry and long, winters harsh, and summers wetter. The average high temperature in 2023 was 9.3°C, and the average low was -0.2°C. It reached a high of 26.7°C on the 27th of July and a low of -21.7°C on the 6th of January.

2.2 Data Collection

In this study, data for air pollutants were obtained from the National City Air Quality Real-Time Publishing Platform (https://air(cnemc).cn:18007/, last access: 31 July 2025), while the China Meteorological Data Service Center provided the meteorological data (http://data.cma.cn, last access: 31 July 2025). There are measurements from atmospheric and meteorological observation stations inside Jilin City, as shown in **Table S1**, together with a background station (FM, Fengman) and six urban stations. The national stations have associated meteorological parameters for air pressure, wind direction, wind speed, and temperature. Data were pretreated in accordance with the Technical Regulation for Ambient Air Quality Assessment to ensure compliance with Ambient Air Quality Standards (AAQS).

The anthropogenic emissions were obtained from the China Multiresolution Emission Inventory (MEIC; http://meicmodel.org/, last access: 11 May 2025), provided by Tsinghua University, with a spatial resolution of 0.25° × 0.25° (Emery et al., 2017; Gao et al., 2021; Li et al., 2017). MEIC has classified emissions into five sectors—industrial, power, transportation, residential, and agriculture—and includes O_3, SO_2, NO_2, $PM_{2.5}$, CO, and VOCs for the regions 70°E–150°E and 10°N–60°N. The Inventory Spatial Allocation Tool (ISAT) disaggregated the emissions spatially, and these are included in the CMAQ model by population density, provincial GDP, and the Chinese Academy of Sciences' land-use data (Wang et al., 2023).

2.3 Model Configuration

The Weather Research and Forecasting (WRF) model (v4.4.1) and the Community Multiscale Air Quality (CMAQ) model (v5.4) were coupled to simulate the temporal and spatial distributions of ground-level O_3 concentrations in proximity to Jilin City, establishing a robust platform for assessing the interactions between meteorological conditions and air quality (Gao and Zhou 2024; Powers et al. 2017; Wang et al. 2021). The details of the parameterization scheme configuration for the WRF-CMAQ model are presented in **Table S2**. WRF was executed utilizing a Lambert Conformal projection and three nested domains for simulations spanning May to July in 2020 and 2023. The Dudhia scheme was employed for shortwave radiation, RRTMG for longwave radiation, Kain–Fritsch for cumulus convection, and the YSU scheme for the planetary boundary layer, incorporating 45 terrain-following vertical layers to accurately represent atmospheric dynamics (Chou et al., 2001; Mlawer et al., 1997; Wang et al., 2023). Additionally, the physics options incorporated the Goddard shortwave scheme, the RRTM longwave model, Purdue Lin microphysics, and the Noah land surface model for surface and boundary-layer processes. Meteorological outputs from WRF were processed using the Meteorology-Chemistry Interface Processor (MCIP). Alongside Initial Conditions (ICON) and Boundary Conditions (BCON), these outputs provided the necessary input for the Community

Multiscale Air Quality (CMAQ) model, where the Chemical Transport Model (CCTM) performed essential chemical and transport simulations. The CMAQ system integrates WRF meteorological fields with the GRID emission inventory to accurately simulate pollutant dynamics and the interactions between meteorology and air quality, as shown in **Figure S1**. To reduce initial-condition bias, the WRF simulation was triggered 5 days in advance. The CMAQ model was utilized for the simulation and verification of O_3 concentrations by determining its aptitude for the simulation of observed trends. A three-level nested domain model was built to ensure appropriate resolution across regional and urban scales, as shown in **Figure 1**. The three domains consisted of the outer 27 km x 27 km domain, including three northeastern provinces of China, the middle 9 km x 9 km domain over the Jilin Province, and the inner 3 km x 3 km domain over Jilin City.

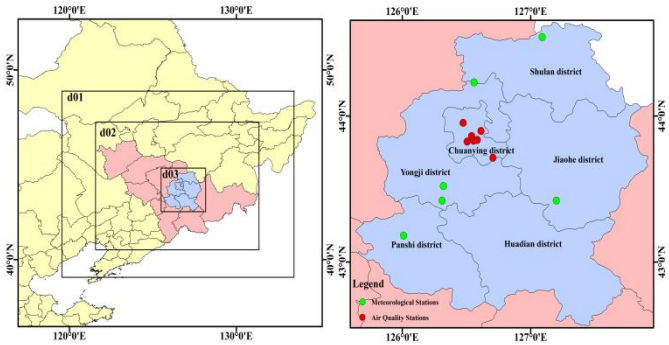

Figure 1. Schematic Illustration of the Nested Modeling Domains Used in This Study over Jilin City, China

The left panel shows the three nested domains, with the outer domain (d01, 27 km × 27 km) covering Northeast China, the intermediate domain (d02, 9 km × 9 km) focusing on Jilin Province, and the innermost domain (d03, 3 km × 3 km) centered on Jilin City. The right panel provides detailed information on the study area, where administrative boundaries are shown together with the distribution of air quality monitoring stations (red dots) and meteorological stations (green dots). This configuration enables accurate evaluation of regional air quality and synoptic weather dynamics, supporting effective environmental modeling and health risk assessment.

The WRF model used Final Analysis (FNL) data from the National Centers for Environmental Prediction (NCEP) for initial conditions, with a temporal resolution of 6 hours and a spatial resolution of 1.0° × 1.0°. For the running of the CMAQ model, the Multiscale Emission Inventory Model of China (MEIC; http://meicmodel.org/, last accessed July 31, 2025), a model by Tsinghua University, provided the gridded fields of emission. Temporal and spatial disaggregation of the inventory was also done by the Spatial Allocation Tools (ISAT).

2.4 Evaluation Indicators

The environmental and meteorological conditions, along with anthropogenic emissions, all play important roles in the generation, dispersion, and transportation of atmospheric pollutants (Zhang et al., 2015). Temperature enhances the vertical convection, and the wind speed and humidity drive the diffusion of the pollutants primarily during storms (Miao, Liao, and Wang 2016; Y. Wang et al. 2022). The season also impacts pollution levels, with colder conditions associated with increased concentrations and stable air masses that accelerate accumulation and long-range transport (Zhao et al., 2014). To account for regional variability in terrain, weather, and emission levels, this work used the WRF model for weather inputs and the CMAQ model to simulate ground-level O_3. Measured data from monitoring stations served for model verification. The quality of model performance was estimated by using R, MFB, MFE, NMB, NME, and RMSE measures, whose criteria for acceptance were defined by reference to (Boylan & Russell 2006; Emery et al., 2017). Results of the simulation were accepted when $-60\% \leq MFB \leq 60\%$, $MFE \leq 75\%$, $NMB \leq \pm 30\%$, $NME \leq 50\%$, and $R > 0.40$. The equations for these statistical markers are explained by (Powers et al. 2017) are given in the supplementary material (Equ. S1-S6).

2.5 Health Assessment

2.5.1 AQI

According to the Ambient Air Quality Standards and the Technical Regulation of the Ambient Air Quality sub-Index(AQI_i) Equations (1,2) can obtain the air quality sub-index of a particular pollutant *i*, and Equation (3) can obtain the total of the pollutant as follows: The sub-index for a specific pollutant can be calculated using Equation (1,2), as stipulated by the Ambient Air Quality Standards (*AAQS*) and the Technical Regulation on the Ambient Air Quality Index. The comprehensive Air Quality Index (*AQI*) for the pollutant is subsequently calculated using Equation (3), as follows:

$$AQI_i = \frac{(AQI_{i,j} - AQI_{i,j-1})}{(Q_{i,j} - Q_{i,j-1})} \times (Q_{i,m} - Q_{i,j}) + AQI_{i,j-1}, j > 1 \quad (1)$$

$$AQI_i = AQI_{i,1} \times \frac{Q_{i,m}}{Q_{i,1}}, j = 1 \quad (2)$$

Thus, since only O_3 is included, the NHAQI is expressed simply as:

$$AQI = AQI_{\mathrm{i}} \quad (3)$$

here indicates pollutant category, *j*, health risk theory; is the measured concentration of the pollutant *i*, and are the upper values of and health risk nearest to the served concentration of the pollutant nd and is the upper limit of concentration in each health risk or nearest to the measured concentration of the pollutant *i*.The classification of AQI ranges, pollutant concentrations, and health effects, as defined by the Ministry of Ecology and Environment of China, is provided in **Table S3**.

2.5.2 Novel Health Risk-Based Air Quality Index (NHAQI)

HAQI was expressed as excess risk of the pollutant (Hu et al., 2015). In this case, the relative risk of the pollutant is calculated as follows:

$$RR_i = exp\left[\beta_i\left(Q_{i,m}\text{-}Q_{i,0}\right)\right],\ Q_{i,m}>Q_{i,0} \quad (4)$$

Where Is the exposure-response relationship coefficient, which specifies the additional health risk per unit increase in the concentration of the pollutant i. For O_3, was measured as 0.048% per 1 μg m^{-3} increase in concentration. The estimated value of the concentration of the pollutant i, $Q_{i,m}$ is observed (monitored), and a concentration of the pollutant i, $Q_{i,0}$ Is the baseline concentration of a pollutant i, i.e., the maximum health concentration level calculated, corresponding to the upper limit of the 24-hour secondary standard **Table S3**. The for pollutant is calculated as follows:

$$ER_i=RR_i\text{-}1 \quad (5)$$

The summation of the ER of the pollutants will be the total ER of the different pollutants, as follows:

$$ER_{Total} = \sum_{i=1}^{n} ER_i = \sum_{i=1}^{n} RR_i \quad (6)$$

(Stieb et al. 2005), set up an arbitrary index, that was bounded between 0 and 10 to measure the excess health risk due to air pollution in his study (Hu et al., 2015) proposed the term $Q_{i,m}$, a level of concentration of the pollutant *i*, equating the associated risk, ER_i, to that of ER_{total}. Nevertheless, using Equation (8) directly to calculate $Q_{i,m}$, may overestimate future direct calculations, and so this paper is the first to work with the new instead of the previous (Ma et al., 2023). To separate the risk levels, a segmentation function was used: where as there is no increase in the health risk caused by the observed concentration of the pollutant *i*, Equation (9) is retained, in contrast, when $Q_{i,m}\geq Q_{i,0}$, and so the health risk caused by the observed pollutant composition is increased Equation (8) is used. Besides, the corresponding relative risk (RR_i^*) of pollutant is calculated as follows:

$$RR_i^*=ER_{total}+1=exp\left[\beta_i\left(Q_{i,m}^*\text{-}Q_{i,0}\right)\right] \quad (7)$$

$$Q_{i,m}^*= \frac{\ln(RR_i^*)}{\beta_i}+Q_{i,0},\ Q_{i,m}>Q_{i,0} \quad (8)$$

$$Q_{i,m}^*= Q_{i,m},\ Q_{i,m}<Q_{i,0} \quad (9)$$

The comparative level of the pollutant *i*, is substituted with the to calculate *NHAQIi*, as shown below:

$$NHAQI_i = AQI_{i,1}\times\frac{Q_{i,m}^*}{Q_{i,1}},\ j=1 \quad (10)$$

$$NHAQI=NHAQI_{\mathrm{i}} \quad (11)$$

Thus, since only O_3 is included, the NHAQI is expressed simply as:

$$NHAQI=NHAQI_{\mathrm{i}} \quad (11)$$

2.6 Scenario Settings

This study used the WRF-CMAQ model to understand how meteorological conditions determined the shift in O_3 levels in Jilin City over the summer seasons of 2020 (May-July) and 2023 (May-July). Both the emission inventory of 2020 and the meteorological data of 2020 were used in the 2020 simulation. In the 2023 simulation, the 2020 emission inventory was used with 2023 meteorological data. This approach will enable an understanding of how meteorological conditions will affect air quality in 2023 through simulation. The details are summarized in **Table 1**.

Table 1. Various Scenarios Were Examined within This Study

Scenarios Name	Meteorological	Emission
Case1	Analysis of the Meteorological Conditions of May-July 2020	Emissions list of 2020
Case2	Analysis of the Meteorological Conditions of May-July 2023	Emissions list of 2020

Note. The table provides a summary of simulation scenarios for May–July 2020 and 2023 meteorological conditions, as well as the 2020 emission inventory, to evaluate atmospheric responses for a sequence of weather patterns.

3. Results

3.1 Model Performance

3.1.1 WRF Model

In this study, the performance of the WRF model simulation was first evaluated by testing the meteorological variables, i.e., 2-meter temperature (T2), 10-meter wind speed (WS10), and 10-meter wind direction (WD10), as summarized in **Table S4, Figure S2**. This model could recreate temporal trends and peak patterns of these parameters. In 2020, the mean simulated temperatures (T2) in May, June, and July were 14.83°C, 20.90°C, and 23.80°C, respectively, with deviations relative to observed temperatures of 0.02°C, 0.60°C, and 0.90°C, underestimates or very slight overestimates.

The correlation coefficient (R) values for T2 and WS10 were both greater than 0.5, indicating a strong correspondence between the simulated data and the observed data. Nonetheless, the value of R for WS10 was still less than that of T2, supporting previous studies that explain the loss of simulation accuracy in wind speed by appreciating the role of the subsurface on surface wind. Performance metrics, such as RMSE, NMB, MFB, NME, and MFE, indicate that the simulation accuracy of all parameters in July 2023 was superior to that seen in July 2020. The reduced performance in 2020 can be attributed to the unstable meteorological conditions of that year.

3.1.2 CMAQ Model

The Community Multiscale Air Quality (CMAQ) model was employed to simulate the ground-based O_3 concentrations in Jilin City during the same periods in 2020 and 2023 that were used in the WRF model (i.e., May, June, and July). Box plots comparing simulated and observed O_3 concentrations in both years are slightly lower than the observed values, as shown in **Figure 2**. For example, the average simulated concentrations in May, June, and July 2020 were 71.95 μg m^{-3}, 75.25 μg m^{-3}, and 76.23 μg m^{-3}, respectively, whereas the measured concentrations were 89.23 μg m^{-3}, 89.25 μg m^{-3}, and 88.91 μg m^{-3}, respectively. Similarly, in May, June, and July 2023, the simulations had values of 91.14 μg m^{-3}, 92.43 μg m^{-3}, and 93.25 μg m^{-3}, respectively; the actual values were 115.10 μg m^{-3}, 114.90 μg m^{-3}, and 118.12 μg m^{-3}, respectively. This reflects a year-on-year growth in simulated data and observed data of approximately 26.7% and 28.9%, respectively, between 2020 and 2023.

To verify model performance, hourly O_3 concentrations at various urban air quality monitoring points were utilized, as shown in **Figure 3**. The model's accuracy varies by month and by year, as shown in **Table 2**. The normalized mean bias (NMB) varied between −29.96% and −23.27% in 2020 and between −30.98% and −22.98% in 2023, reflecting steady underestimation of the O_3 levels. The normalized mean error (NME) varied between 36.32% and 45.06% in 2020 and between 35.61% and 41.68% in 2023, showing a moderate level of improvement. Regardless of the bias, the model reproduced seasonal and yearly patterns faithfully.

Similarly, in 2023, correlation coefficients (R) between model results and observational O_3 concentrations increased in certain months by up to 0.70 at selected stations—the sign of a moderate to satisfactory agreement. Mean fractional bias (MFB) and mean fractional error (MFE) for all the sites stayed inside the accepted limits (−60% ≤ MFB ≤ 60%, MFE ≤ 75%), validating the model for further study. Nonetheless, stations HDW and DJZ showed elevated biases where the normalized mean bias (NMB) was higher than 30% for certain months, indicating underestimates of the peak levels of O_3. These biases are most likely due to the uncertainties of the precursors that are emitted (VOC and NO_x), the coarse resolution of the emission data, and the difficulties in simulating the meteorological parameters, like the boundary layer height, temperature, and radiation. The model, CMAQ, showed fair performance in representing the seasonal and interannual patterns of O_3 in Jilin City.

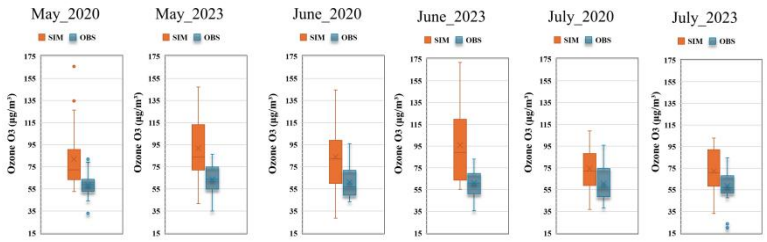

Figure 2. Box Plots of the Mean Day-to-day Ozone (O_3) Concentrations (μg m^{-3}) in the City of Jilin for May–July 2020–2023 for OBS versus SIM

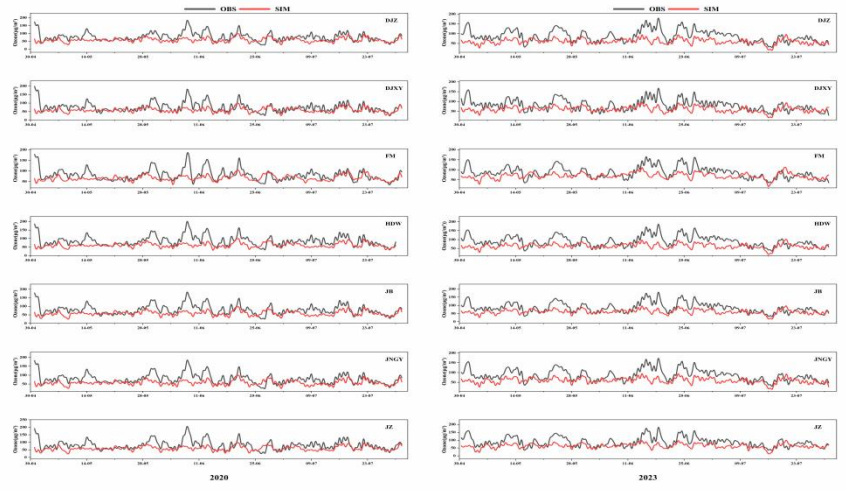

Figure 3. Simulated ozone (O_3) concentrations by the CMAQ model across the observation stations in Jilin City for May–July 2020 (left panels) and 2023 (right panels) by comparison between observed data (OBS) and simulation outcomes (SIM). Locations are Hada Bay (HDW), East Bureau (DJZ), Electric Power College (DJXY), Jiangnan Park (JNGY), Fengman Control (FM), and Jiuzhan (JZ)

Table 2. Error statistics of Simulated ozone (O_3) concentrations compared with observations from air quality monitoring stations in Jilin City during May–July of 2020 and 2023

Monitoring Sites	Statistical Indicators	May-2020	May-2023	June-2020	June-2023	July-2020	July-2023
HDW	Simulated Mean Value	59.75	65.00	62.09	67.20	61.8	59.86
	Monitoring Mean Value	85.31	94.18	91.142	100.34	80.63	77.72
	R	0.39	0.41	0.51	0.65	0.63	0.54
	NMB	29.96%	30.98%	31.88%	33.02%	23.27%	22.98%
	NME	36.32%	41.68%	45.06%	41.37%	37.14%	35.61%
	MFB	30.30%	31.73%	31.47%	29.81%	16.67%	26.25%
	MFE	41.59%	53.09%	58.76%	49.66%	44.90%	45.36%
	RMSE	43.13	46.90	53.06	54.05	41.25	34.38
DJZ	Simulated Mean Value	57.13	61.96	59.79	63.92	58.12	56.15
	Monitoring Mean Value	78.58	92.70	83.51	97.77	72.37	72.37
	R	0.44	0.53	0.56	0.63	0.37	0.58
	NMB	27.29%	33.09%	28.40%	34.61%	19.68%	22.41%
	NME	35.59%	40.01%	42.10%	40.73%	33.21%	36.01%
	MFB	28.17%	37.98%	28.95%	36.06%	17.46%	28.88%
	MFE	42.41%	52.22%	55.51%	49.23%	41.42%	48.20%

	RMSE	39.25	45.27	45.45	51.49	32.56	32.30
	Simulated Mean Value	58.02	63.50	58.23	64.07	58.10	55.58
	Monitoring Mean Value	78.9	88.66	77.88	86.46	68.80	67.72
	R	0.41	0.51	0.61	0.68	0.70	0.56
DJXY	NMB	26.38%	29.12%	22.73%	25.89%	15.55%	17.94%
	NME	41.38%	43.20%	45.99%	44.07%	38.72%	38.53%
	MFB	19.60%	25.88%	12.08%	10.08%	1.01%	18.54%
	MFE	49.94%	55.88%	62.34	58.46%	51.26%	50.44%
	RMSE	44.15	46.44	46.32	49.78	34.65	32.73
	Simulated Mean Value	56.33	61.03	59.02	63.27	56.73	55.13
	Monitoring Mean Value	83.40	91.77	83.06	96.37	71.30	71.66
	R	0.43	0.53	0.56	0.63	0.70	0.59
JNGY	NMB	32.06%	33.49%	28.95%	34.35%	20.44%	23.07%
	NME	37.48%	40.32%	42.78%	40.46%	32.15%	36.14%
	MFB	37.20%	39.86%	29.61%	37.40%	20.58%	30.75%
	MFE	45.14%	54.13%	58.06%	49.75%	41.92%	50.35%
	RMSE	42.90	45.02	46.50	51.38	31.20	32.27
	Simulated Mean Value	63.70	68.75	68.86	74.47	66.83	66.40
	Monitoring Mean Value	83.17	91.18	84.48	96.76	72.39	71.54
	R	0.28	0.34	0.46	0.62	0.61	0.41
FM	NMB	23.41%	24.56%	18.48%	23.04%	7.69%	7.20%
	NME	33.78%	35.09%	37.70%	36.50%	28.20%	35.38%
	MFB	20.58%	24.91%	12.66%	16.17%	2.67%	3.83%
	MFE	35.65%	42.56%	42.47%	39.74%	30.44%	39.97%
	RMSE	40.04	40.81	42.46	46.09	26.83	32.30
	Simulated Mean Value	57.99	63.06	60.14	66.71	60.67	59.45
	Monitoring Mean Value	82.71	92.78	84.16	95.17	78.18	74.23
	R	0.42	0.49	0.53	0.64	0.66	0.54
JZ	NMB	29.88%	32.03%	28.55%	29.90%	22.39%	19.92%
	NME	39.43%	45.36%	49.43%	43.75%	40.59%	37.44%
	MFB	30.99%	32.03%	21.76%	19.70%	10.21%	19.69%
	MFE	48.10%	61.78%	68.57%	54.21%	52.57%	49.67%
	RMSE	44.22	49.89	53.20	53.41	40.73	34.65
	Simulated Mean Value	57.39	62.44	59.25	65.01	58.88	57.41
	Monitoring Mean Value	80.98	90.51	83.74	97.56	74.35	70.58
	R	0.43	0.52	0.57	0.67	0.67	0.58

JB	NMB	29.14%	31.01%	29.24%	33.36%	20.80%	18.67%
	NME	37.85%	39.72%	42.74%	40.81%	32.37%	35.92%
	MFB	30.71%	33.89%	32.60%	32.87%	19.81%	20.97%
	MFE	45.00%	51.98%	57.79%	48.68%	38.42%	46.34%
	RMSE	41.64	44.48	46.93	51.59	32.85	32.25

Note: Statistical comparison between CMAQ model-simulated ozone (O_3) levels and measurements at seven monitoring sites in Jilin City—Hada Bay (HDW), East Bureau (DJZ), Electric Power College (DJXY), Jiangnan Park (JNGY), Fengman Control (FM), Jiuzhan (JZ), and Jiangbei (JB)—in the summer of 2022 and 2023. Parameters are model-simulated and observed mean values, normalized mean bias/error (NMB, NME), mean fractional bias/error (MFB, MFE), and root mean square error (RMSE), which show model performance between years.

3.1.3 Meteorological Influences on Ozone Dynamics

To investigate the influence of meteorological parameters on O_3 concentrations, this study compares yearly variations between 2020 and 2023 based on key meteorological variables, including 2-meter temperature (T2), 10-meter wind speed (WS10), surface air pressure, and planetary boundary layer height (PBLH). **Figure 4(a)** depicts the average temperature in May was 14.2°C in 2020 compared to 15.5°C in 2023, meaning that in 2023, the temperature rose by 1.3°C. Likewise, the temperature in June increased by 1.5°C since the preceding year (15.1°C in 2020 vs 16.6°C in 2023), whereas the July temperature increased by 1.1 °C (23.6°C in 2020 vs. 24.7°C in 2023). These warming trends suggest that elevated temperatures in 2023 may have contributed to an increase in photochemical O_3 production, as higher temperatures are known to enhance reaction rates. **Figure 4(b,c)** reveals notable variations when comparing monthly wind speed between 2020 and 2023. Throughout June 2020, the wind speed fluctuated between 1.70 m s^{-1} and 7.34 m s^{-1}, whereas in June 2023, the variation was a bit more, between 1.62m s^{-1} and 7.23 m s^{-1}. In July, the wind speed ranged from 1.48 m s^{-1} to 5.71 m s^{-1} in 2020, whereas it was in the range of 1.95 m s^{-1} to 5.84 m s^{-1} in 2023. These values indicate that there is an apparent variation between one year and another, suggesting a fluctuation in wind behavior. Still, there is no clear direction of either rising or declining wind strength throughout the months being studied. It is interesting to note that in May 2023 (10.64 m s^{-1}) and July 2023 (5.84 m s^{-1}), extreme wind events were observed. In contrast, the minimum wind speeds were recorded on average in July 2020 at 1.48 m s^{-1}. These variations in wind dynamics can severely affect the diffusion of air pollution, leading to changes in its spatial and temporal distribution across seasons and years.

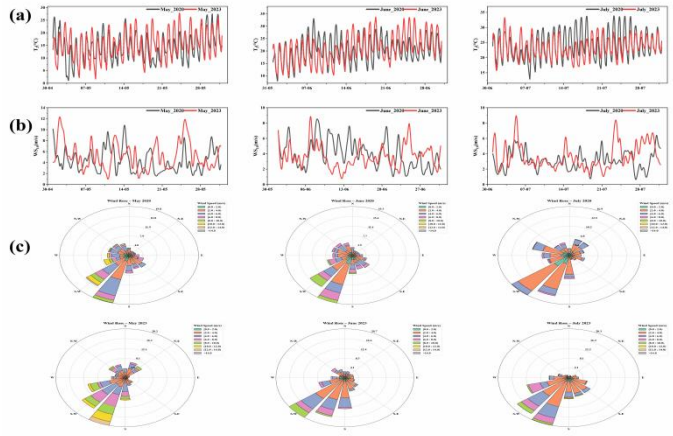

Figure 4. Distributions of 2-meter Temperature (T2) (a), 10-meter Wind Speed (WS10) (b), and Wind Direction (c) in Jilin City during May–July between 2020 and 2023. Hourly Variation for panels (a) and (b) and wind rose Charts for Directional and Frequency Patterns for Panel (c)

Extended high-pressure systems exceeding 950 hPa were related to high O_3 episodes from May 25–31, 2023 (953–961 hPa), and June 10–16, 2020 (as high as 954.3 hPa), as shown in **Figure 5**. Such conditions inhibit atmospheric mixing by subsidence inversion, restricting the vertical dispersion and favoring surface-level accumulation of O_3 and its precursors. A comparison of planetary boundary layer height (PBLH) between the two years is shown in **Figure 5**. The average PBLH in May 2020 stood at 734.5 m but fell to 762.9 m in May 2023 (−3.3%). Greater decreases occurred in July 2023 when PBLH fell to 158.8 m on the 15th and 280.3 m on the 24th, during the period of highest O_3 concentrations. Low boundary layers during these instances restrict vertical mixing, exacerbating O_3 accumulation.

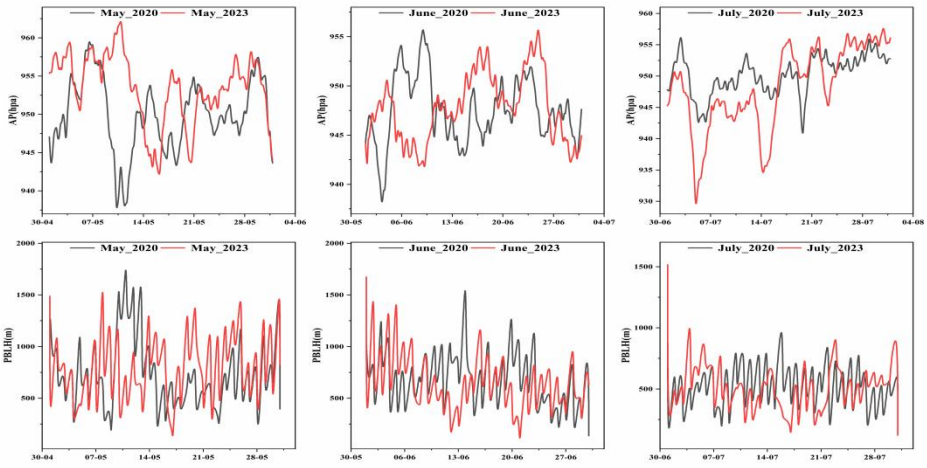

Figure 5. Distribution of air pressure (AP) and planetary boundary layer height (PBLH) patterns over Jilin City during May–July of the years 2020–2023. The top panels show the day-to-day change of AP (hPa), and the bottom panels show the PBLH patterns (m) for the seasonal and interannual meteorological dynamics forming O_3

3.2 Spatiotemporal Variations of AQI and NHAQI in Summer

The average monthly ground-level O_3 concentrations observed at seven state-controlled monitoring stations in the city of Jilin in May, June, and July of 2020 and 2023 are shown in **Figure 6**. The results show a significant decline in O_3 levels during May 2023 as compared to May 2020. For example, Fengman experienced a reduction from 183.03 μg m^{-3} in 2020 to 94.87 μg m^{-3} in 2023 (−48.2%), Jiuzhan dropped from 167.47 μg m^{-3} to 109.13 μg m^{-3} (−34.8%), and Jiangbei decreased from 165.47 μg m^{-3} to 105.03 μg m^{-3} (−36.5%). Other stations also observe similar declining trends, such as Jiangnan Park (−36.1%) and East Bureau (−40.2%).

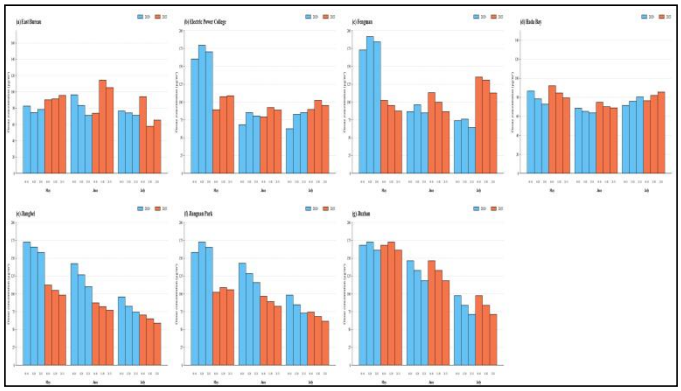

Figure 6. Monthly Average Ozone (O_3) Concentrations (μg m^{-3}) at Seven Monitoring Sites in Jilin City—Hada Bay (HDW), East Bureau (DJZ), Electric Power College (DJXY), Jiangnan Park (JNGY), Fengman Control (FM), Jiuzhan (JZ), and Jiangbei (JB)—during May–July of 2020 and 2023

The Air Quality Index (AQI) was calculated from the average O_3 concentrations measured at seven monitors covering the prefecture-level city of Jilin City, providing a quantitative assessment of summer air quality. Summer O_3 pollution increased significantly, such that the mean AQI increased from 40.62 in 2020 to 46.22 in 2023 (May–July). The highest O_3 episodes occurred on June 8, 2020, at Jiuzhan station (AQI 192, Unhealthy), and on June 19, 2023, at Hada Bay station (AQI 170, Unhealthy). The number of "good" days (AQI 51–100) reduced from 82 (89.1%) in 2020 to 77 (83.7%) in 2023, but "moderate" pollution days (AQI 101–150) increased from 18 to 26, as shown in **Figure 7**. Days under the "unhealthy for sensitive groups" level (AQI 151–200) increased from 5 to 8, but the "unhealthy" pollution days (AQI 201–300) stayed unchanged at 2 for both years.

The maximum O_3 levels in the two summers also fell in the last week of June and the first week of July when temperatures (T2) were elevated, surface pressure was higher, and planetary boundary layer height (PBLH) was lower, as shown in **Figure 8**. Lower wind speeds (WS10) and stable wind direction also limited dispersion and enabled the accumulation of pollutants in 2020. The very opposite conditions prevailed in 2023 when stronger and variable winds enhanced atmospheric ventilation and limited extreme O_3 formation. It appears that the interannual variability of summer O_3 pollution in Jilin

City is insensitive to synoptic dispersion and vertical mixing.

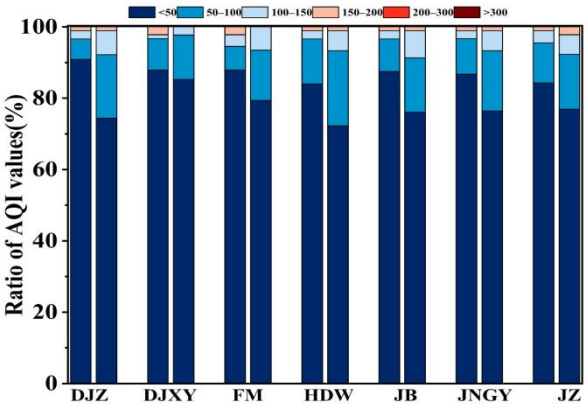

Figure 7. Percentage of Days for Six AQI Health Categories for Seven Stations of the City of Jilin City—Hada Bay (HDW), East Bureau (DJZ), Electric Power College (DJXY), Jiangnan Park (JNGY), Fengman Control (FM), Jiuzhan (JZ), and Jiangbei (JB)—during the months of May–July 2020 and 2023

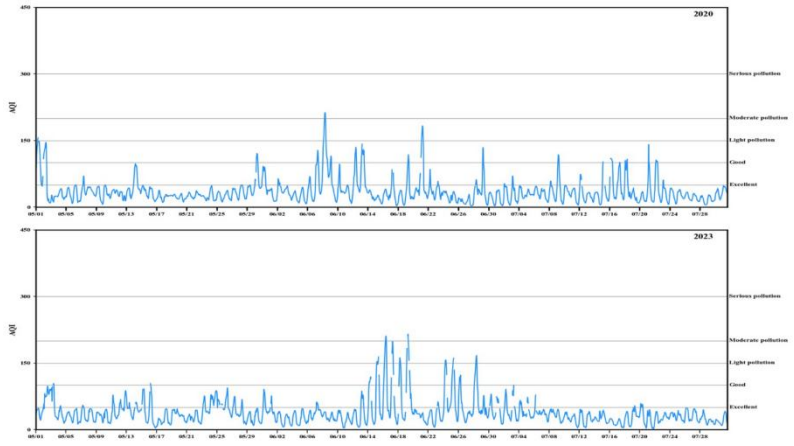

Figure 8. Hourly variation of the Air Quality Index (AQI) in Jilin City for May–July 2020 and 2023. The top panel corresponds to the variation of the AQI in 2020, and the bottom panel corresponds to the variation in 2023. Horizontal reference lines represent the AQI health levels: Good, Moderate, Unhealthy, and Hazardous, and emphasize temporal changes in the level of pollution

The Normalized Health-based Air Quality Index (NHAQI) designed here provides a health-sensitive estimate of exposure to O_3 pollution that is superior to the traditional AQI overall, particularly for May–July in 2020 and 2023 in the City of Jilin. For values of AQI below 50, NHAQI signaled no undue health risk. With higher levels of pollution, NHAQI afforded a finer grading of health effects as shown in **Figure 9**. For moderate pollution ($50 < AQI \leq 100$), 78 and 22 days for 2020 and 2023, respectively, were classified by the NHAQI as Satisfactory and Moderate, versus 82 and 18 for 2023 versus 2020—a small reduction. For moderate AQI levels ($100 < AQI \leq 150$), the proportion of days classified as moderate by the NHAQI increased from 67% in 2020 to 76% in 2023, while reducing poor

classifications to indicate a shift towards lower intensity. However, for serious pollution (150 < AQI ≤ 200), Very Poor NHAQI day percentages rose from 15% in 2020 to 38% in 2023, indicating rising higher-risk periods. For days when the AQI jumped above 200, the NHAQI always categorized them as "poor" or "destitute," signaling significant health issues. Overall, the NHAQI enhances air quality interpretation by shifting the emphasis to the health impact, indicating some decreases in some categories but an increase in extreme pollution days—with a flag for future vigilance and locationally targeted controls.

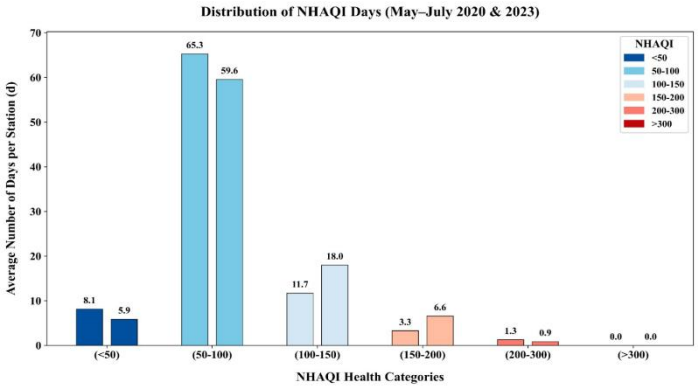

Figure 9. Distribution of the number of NHAQI days for six AQI health categories of Jilin City during May–July 2020 and 2023. Health categories are the levels of AQI <50, 50–100, 100–150, 150–200, 200–300, and >300 for the mean number of days per station for their respective associated air quality levels

Seasonal average Normalized Health-based Air Quality Index (NHAQI) showed spatial and temporal dissimilarity in summer air pollution O_3 in these six administrative districts of Jilin City (Huadian, Yongji, Chuanying, Jiaohe, Panshi, and Shulan), as shown in **Figure 10, Table S5**. The seasonal mean NHAQI has worsened in 2023, rising to 90.9 (May-July) compared with 82.4 (May-July) in 2020, indicating an aggravation of air quality. Urban areas like Huadian (117.5), Yongji (97.6), and Chuanying (108.6) had higher values, and the lowest June mean was measured at Panshi (110.6). In contrast, Jiaohe (122.2) and Shulan (105.6) exhibited relatively high values, suggesting regional pollutant transport. The concentration of severe O_3 episodes was concentrated in June, with the peak of June 19, 2023, in Jilin (204.38) and Jiaohe (171.19), and June 8, 2020, in Shulan (226.70) and Panshi (280.64). These episodes were tracked to intense solar radiation and high temperatures (~24°C) and low PBLH (~505m), which constrained the atmospheric dispersion, whereas the June PBLH values were relatively higher (e.g., Jiaohe: 643.82 m), leading to lower NHAQI in some districts. The patterns reveal the combined role of city emissions and weather (meteorological) conditions, where June is especially limited in terms of O_3 accumulation due to stagnant air and increased photochemical reactions.

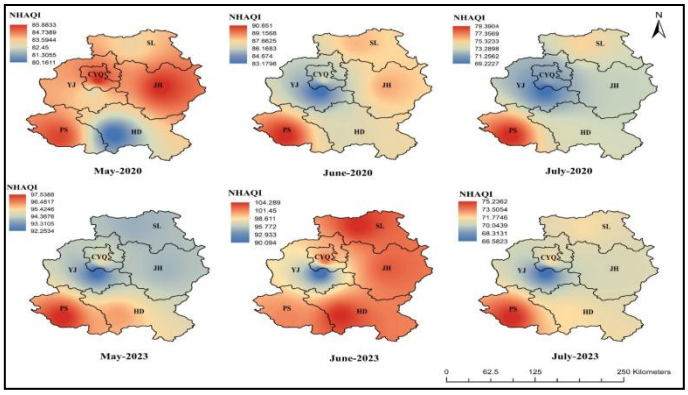

Figure 10. Spatial distribution of NHAQI in districts of Jilin City from May to July in 2020 and 2023. Shulan (SL), Jiaohe (JH), Huadian (HD), Panshi (PS), Yongji (YJ), and Chuanying (CYQ) are the districts. Color gradients indicate levels of the NHAQI to show temporal and spatial variation in air quality

The overall excess risk (ER_{total}) for O_3 exposure for seven monitoring stations in Jilin City in May–July 2020 and 2023 is shown in **Figure 11**. The city average ER_{total} was 2.19% in 2020, the lowest reading being from East Bureau (2.05%), and the values higher than the average being Hada Bay 2.4% and Jiuzhan and Fengman (2.2% each). The value in 2023 slightly decreased to 2.13% for ER_{total}, indicating moderate success in controlling O_3. Reductions were noted at most stations, while Hada Bay remained unchanged, and both Hada Bay and Jiuzhan again showed values above the city average at 2.3% and 2.15%, respectively. These results highlight current spatial heterogeneity in summer O_3-linked health impacts, with some locations experiencing long-duration exposure throughout the summer season. The study also highlights the need for location-specific reduction strategies to counter spatially resolved O_3 pollution and its impacts.

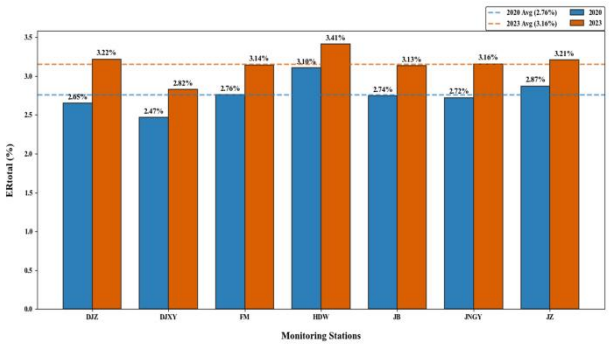

Figure 11. Average ER_{total} values recorded in May–July 2020 and 2023 for seven air quality monitoring stations in the city of Jilin City—East Bureau (DJZ), Electric Power College (DJXY), Fengman Control (FM), Hada Bay (HDW), Jiangbei (JB), Jiangnan Park (JNGY), and Jiuzhan (JZ). Blue bars represent the values for 2020, and orange bars represent the values for 2023. Dotted lines represent the yearly averages

4. Discussion

The model's performance showed that WRF simulated temperature well ($R > 0.8$, low bias < 1°C), but it had lower skill in predicting surface winds. In contrast, CMAQ shows an underprediction bias during peak O_3. Even though the model realistically predicted the seasonality and the interannual variability. The outcome is consistent with previous evaluations of the WRF–CMAQ model's performance during complex urban extremes, where the spatial variability of meteorological heterogeneity inhibits the accurate simulation of wind and turbulence (Chen et al. 2017; Powers et al. 2017) . A pronounced signal from our research found an amplified mean warming from 2020 to 2023, driven by a 1.3°C increase in May, equivalent to increased O_3. The result is consistent with the photochemical hypothesis, indicating that hot periods hasten NOx–VOC reaction rates and are responsible for enhanced O_3 formation, whereas shallow boundary layers confine pollutants closer to the ground (P. Wang et al. 2022; Zhao et al. 2021) . Warmth increases the rates of photochemical processes and alters the partitioning of VOC–NO_x toward increased O_3 formation. (Bao et al. 2025) determined that the O_3–temperature sensitivity above China is one of the biggest over the globe, equivalent to an approximately 2.9 μg m^{-3} $°C^{-1}$ climate penalty coefficient. The process illustrates the role of warmth in the amplified growth of O_3 observed over Jilin City. Analogously, the relationships between temperature and O_3 have been defined above other eastern Chinese regions, where amplified warming offsets radical chemistry and extends daytime O_3 longevity (Gao et al., 2020; Yang et al., 2019). Our findings indicated that enduring high-pressure systems and stagnant weather conditions substantially contributed to increased O_3 levels, particularly in late May 2023 and June 2020. Extended anticyclonic circumstances are acknowledged for diminishing vertical mixing, obstructing horizontal advection, and promoting the accumulation of O_3 and its precursors. (Su, Jiao, & Xu 2025) revealed that combined heatwave and high-pressure systems exacerbate O_3 pollution in China by intensifying photochemical reactions and restricting dispersion. The mechanism aligns with the stagnation observed in Jilin City, where high-pressure systems over 950 hPa are associated with substantial increases in O_3 concentrations.

Boundary layer dynamics had a significant impact on O_3 levels. Shallow planetary boundary layer heights (PBLH) have been linked to elevated precursor concentrations and O_3 accumulation, as shallow PBLH prevent upward dispersion and keep pollutants near the surface. Our simulations uncovered minima in PBLH around 158.8 m and 280.3 m during the high-O_3 days, settings suitable for pollutant accumulation. (Zhang et al., 2023) discovered that Beijing had a nonlinear relationship between planetary boundary layer height and the level of O_3 found by the level of PBLH, where the moderate PBLH favors the vertical mixture as well as the high O_3 concentrations, but very shallow layers overstate the accumulation. (Liao et al., 2024) stipulated that the upper limit of the mixing layer is usually an impediment dividing surface-based O_3 from the free troposphere; thus, where the layer is suppressed, the O_3 is entrapped below. The interrelation between temperature and radiation, as well as boundary-layer dynamics, provides an unequivocal account of the interannual variation in O_3 levels.

Wind speed and direction also affected local O_3 patterns. The changing wind regime during 2023 enabled the ventilation during some episodes but stagnation during the rest. Light winds and steady directions facilitated the accumulation of the oxidant in emission-dense subdistricts, such as Hada Bay and Jiuzhan. The heavier and variable wind flows facilitated the dispersion of the pollutant. The persistence of these hotspots was further influenced by local terrain features, which reduced dispersion and prolonged the stagnation of O_3 plumes (Chen et al., 2021). The same pattern has been observed in other Chinese cities, where changes in wind persistence determine whether O_3 episodes are locally photochemically or regionally transport-dominated (She et al., 2024). The regional background O_3 in China is approximately 81% of the daily 8-hour maximum, suggesting that local changes often reflect superimposed background levels conditioned by weather (Sun et al., 2024). This clarifies the spatial correlation of O_3 across stations in the Jilin region, despite changes in local emissions.

The systematic underestimation of O_3 by CMAQ identified in this study highlights established limitations of emission inventories and chemical mechanisms. The incomplete representation of reactive VOC species and biases in VOC–NO_x ratios may lead to an underestimation of simulated peak O_3 levels. (She et al., 2024) highlighted that the underestimation of VOC emissions is the primary factor contributing to the low O_3 bias observed in current regional models. Further, (Wu et al., 2024; Zheng et al., 2018) also noted that the MEIC inventory, despite being extremely popular for its application over broad regions, underestimates the emissions from the chosen sectors, like the application of solvents and industrial VOCs, and also lacks the spatial detail to delineate the complexities of the complex urban sources. The 0.25° MEIC data set used herein would most likely have smoothed over the emission hotspots, resulting in a suppressed signal over the O_3 peaks.

The Normalized Health-based Air Quality Index (NHAQI) introduction provides an enhanced health-based risk evaluation for O_3. The citywide excess risk (ER_{total}) fell marginally from 2.19% to 2.13%. Yet, the upward trend in high-severity NHAQI days indicates an escalation of acute health risk, even with a slight reduction in average exposure. The discrepancy reflects average exposure measures that may obscure localized or episodic health burdens. The study by (Du et al., 2024) that took place nationwide in China found that co-exposure to O_3 and to heatwaves greatly increases the risk of death, thereby confirming the fact that the episodic O_3 acutely prescribes robust health effects. The repeated occurrence of the hotspots within the industrial areas, for example, Hada Bay and Jiuzhan, also complements the findings within the Pearl River Delta, whereby the risk of exposure is expedited with the localized robustness and magnitude of the emissions and the associated topographic effects (Chen et al., 2021). Accordingly, the pointwise regulation of NO_x and reactive VOC emissions is a paramount policy imperative.

The insignificant improvement in city averages, along with localized degradation, suggests that mitigation and adaptation approaches should focus on areas prone to stagnation. The use of meteorological indices, such as boundary-layer depth, temperature, and stagnation occurrence, to augment real-time O_3 forecasts strengthens early warnings and guides transient emission controls. The

coupling of meteorological and air-quality forecasting in real-time, presented by (Yang et al., 2025) and reviewed by (Sokhi et al., 2022), significantly strengthens the accuracy of O_3 forecasting and enhances public health communication for episodes with serious air quality. Despite the progress made, certain limitations remain. The coarse spatial resolution of the MEIC inventory and its application for post-2020 emissions likely leads to an underestimation of actual changes following pandemic recovery. Quality uncertainties in the WRF wind simulation result in errors during dispersion analysis. The present study dealt exclusively with O_3, excluding co-pollutants like $PM_{2.5}$ and NO_2, which have been shown to have synergistic health effect (Cromar et al., 2020). Comparing only two summers makes it difficult to distinguish between changes driven by emissions and those driven by meteorology. Future studies need to extend the time series, include observational VOC and NO_x data to improve inventories, and utilize source-apportionment or tagged-tracer methods to resolve contributions from regional versus local sources. High-resolution emission data sets (Wang et al., 2023) and receptor-based approaches allow better quantification of source contributions from the biogenic, industrial, and traffic sectors. Health impact studies that include multiple pollutants, such as the present study, which includes O_3, $PM_{2.5}$, and NO_2, will allow for a better understanding of atmospheric health risks. Inter-city cooperation over Northeast China is vital to estimate the accuracy of the emission inventories better, standardize the monitoring networks, and materialize consistent cross-region mitigative strategies (Hou et al., 2020).

This study demonstrates that O_3 pollution in Jilin City is jointly influenced by meteorological variability and emission patterns. The synergistic effects of rising temperatures from westward airflows, shallower planetary boundary layer heights, and stable atmospheric circulations create favorable conditions for enhanced photochemical O_3 production. However, current emission control measures have not fully mitigated the amplifying effects of weather on O_3 levels. Effective management of O_3 pollution and its health consequences in Northeast China, therefore, requires continuous and integrated efforts involving persistent air quality monitoring, refinement of emission inventories for greater spatial and temporal accuracy, and development of coordinated meteorology-chemistry forecasting systems that can anticipate pollution episodes and guide timely interventions. However, this analysis has some limitations. The emission inventory spatial resolution employed (MEIC at 0.25°) is relatively coarse and is likely to smooth critical emission hotspots, leading to the underprediction of peak O_3 levels. The simulation also relied on 2020 emission levels for the 2023 model, which are unlikely to capture changes during the post-pandemic period, thereby diminishing the potential to separate meteorological from emission-driven effects. Meteorological simulation uncertainties, especially in wind speed and planetary boundary layer behavior, introduce errors that compromise the accuracy of pollutant dispersion modeling. The analysis focused solely on O_3, excluding co-pollutants $PM_{2.5}$ and NO_2, hindering the assessment of joint health effects. Finally, comparing only two summers limits knowledge of longer-term trends and interannual variability.

Looking ahead, greater priority should be placed on the design and implementation of high-resolution, current emission inventories that incorporate recent anthropogenic and biogenic changes and are tested with comprehensive in situ measurements of NOx and VOCs. Expanded multi-pollutant modeling, encompassing $PM_{2.5}$, NO_2, and O_3, will enable an integrated analysis of air quality and health risks. Advanced source apportionment and tagged-tracer methods can help to elucidate the relative importance of local and regional emissions, enabling targeted policy interventions. Advanced meteorology-chemistry coupled forecasting models with real-time data assimilation will better capture air pollution episodes and deliver health risk communication. Inter-regional coordination at the regional level across Northeast China is necessary to standardize monitoring networks, facilitate enhanced information sharing, and implement regionally synchronized mitigation strategies that account for the cross-regional transport of air pollutants. Lastly, long-term observational studies will more effectively distinguish between emission- and meteorology-driven O_3 changes, providing a firmer foundation for planning and implementing air quality management. A comprehensive strategy that combines state-of-the-art modeling, monitoring, and cross-regional collaboration is crucial for reducing O3 air pollution and protecting public health in Jilin City and the broader Northeast China region.

5. Conclusion

This study integrates observational datasets and health risk analyses to validate the capacity of the WRF and CMAQ models to simulate meteorological variables and ground-level O_3 levels over the city of Jilin during the summers of 2020 and 2023. While the WRF model robustly captured temperature patterns ($R > 0.8$, bias $< 1°C$), it did not adequately model surface wind, especially for 2020. The CMAQ model reproduced the overall oxidant trends but consistently underpredicted peak O_3 levels, suggesting uncertainties in meteorological forcing and emissions inventories. The otherwise tightly coupled modeling system, however, successfully demonstrated the impacts of major climatic factors—namely, temperature, wind kinematics, and boundary layer height—on O_3 variability, meeting corresponding statistical performance requirements. Health hazards associated with O_3 were widespread during the study period, with the decrease from 2020 to 2023 being only modest, underscoring the need for localized mitigation measures. The model parameterizations need to be strengthened through future advancements, and the emissions datasets need to be corrected to higher spatial and temporal resolutions. Urban-scale policies also need to be integrated at an enhanced spatial detail. The comprehensive model framework provides the scientific underpinnings for evidence-based management practices to mitigate O_3-related health hazards.

Acknowledgments

The authors sincerely thank the members of Laboratories 537 and 142 at Jilin University for their valuable assistance and guidance throughout this study. Appreciation is also extended to the MEIC team at Tsinghua University for providing the Multiscale Emission Inventory of China (MEIC). The

authors would also like to gratefully acknowledge the anonymous reviewers for their valuable contributions in improving the quality of the manuscript. All authors have reviewed and approved the final manuscript and take full responsibility for its content.

Credit authorship contribution statement

Anees Akhtar: Writing – review and editing, Conceptualization, Resources, and Methodology. **Chunsheng Fang:** Review and editing, Supervision, and Resources. **Muhammad Yousuf Jat Baloch:** Review, editing, and Proofreading. Validation and Software. Proofreading, Software Development, and Data Curation. **Ju Wang:** Data curation. Software, Data curation, and Visualization. Formal analysis and Visualization. Review, editing, and Proofreading. Validation and Software. Proofreading, Software Development, and Data Curation.

Data Availability

The data will be provided to the corresponding author upon request.

Ethics Approval

Not applicable.

Consent to Participate

All authors reviewed and approved the final manuscript.

Competing Interests

The authors declare no competing interests.

References

Ashworth, K., Wild, O., & Hewitt, C. N. (2013). Impacts of biofuel cultivation on mortality and crop yields. *Nat Clim Chang*, *3*(5). https://doi.org/10.1038/nclimate1788

Bai, L., Li, C., Yu, C. W., & He, Z. (2021). Air pollution and health risk assessment in northeastern China: A case study of Jilin Province. *Indoor Built Environ*, *30*(10). https://doi.org/10.1177/1420326X20979274

Bao, J., Li, X., Kong, L., Li, J., Chen, Q., & Zhang, Y. (2025). Comparative analysis of the impact of rising temperatures on ozone levels in China and the United States. *Npj Clean Air*, *1*(1). https://doi.org/10.1038/s44407-025-00023-8

Bell, M. L., Peng, R. D., & Dominici, F. (2006). The exposure-response curve for ozone and risk of mortality and the adequacy of current ozone regulations. *Environ Health Perspect*, *114*(4), 532-536. https://doi.org/10.1289/ehp.8816

Boylan, J. W., & Russell, A. G. (2006). PM and light extinction model performance metrics, goals, and

criteria for three-dimensional air quality models. *Atmos Environ*, *40*(26). https://doi.org/10.1016/j.atmosenv.2005.09.087

Chen, D., Xie, X., Zhou, Y., Lang, J., Xu, T., Yang, N., Zhao, Y., & Liu, X. (2017). Performance evaluation of the WRF-Chem model with different physical parameterization schemes during an extremely high PM2.5 pollution episode in Beijing. *Aerosol Air Qual Res*, *17*(1). https://doi.org/10.4209/aaqr.2015.10.0610

Chen, S. P., Liu, W. T., Hsieh, H. C., & Wang, J. L. (2021). Taiwan ozone trend in response to reduced domestic precursors and perennial transboundary influence. *Environ Pollut*, *289*, 117883.

Chen, X., Wang, N., Wang, G., Wang, Z., Chen, H., Cheng, C., Li, M., Zheng, L., Wu, L., Zhang, Q., Tang, M., Huang, B., Wang, X., & Zhou, Z. (2022). The influence of synoptic weather patterns on spatiotemporal characteristics of ozone pollution across Pearl River Delta of southern China. *J Geophys Res Atmos*, *127*(21). https://doi.org/10.1029/2022JD037121

Chou, M. D., Suarez, M. J., Liang, X. Z., Yan, M. M. H., & Cote, C. (2001). *A thermal infrared radiation parameterization for atmospheric studies* (No. NASA/TM-2001-104606/VOL19).

Cromar, K. R., Ghazipura, M., Gladson, L. A., & Perlmutt, L. (2020). Evaluating the U.S. air quality index as a risk communication tool: Comparing associations of index values with respiratory morbidity among adults in California. *PLoS ONE*, *15*(11). https://doi.org/10.1371/journal.pone.0242031

Du, H., Yan, M., Liu, X., Zhong, Y., Ban, J., Lu, K., & Li, T. (2024). Exposure to concurrent heatwaves and ozone pollution and associations with mortality risk: A nationwide study in China. *Environ Health Perspect*, *132*(4), 047012-1–047012-10. https://doi.org/10.1289/ehp13790

Emery, C., Liu, Z., Russell, A. G., Odman, M. T., Yarwood, G., & Kumar, N. (2017). Recommendations on statistics and benchmarks to assess photochemical model performance. *J Air Waste Manag Assoc*, *67*(5). https://doi.org/10.1080/10962247.2016.1265027

Gao, L., Liu, Z., Chen, D., Yan, P., Zhang, Y., Hu, H., Liang, H., & Liang, X. (2021). GPS-ZTD data assimilation and its impact on wintertime haze prediction over North China Plain using WRF 3DVAR and CMAQ modeling system. *Environ Sci Pollut Res*, *28*(48). https://doi.org/10.1007/s11356-021-15248-9

Gao, M., Gao, J., Zhu, B., Kumar, R., Lu, X., Song, S., Zhang, Y., Jia, B., Wang, P., Beig, G., Hu, J., Ying, Q., Zhang, H., Sherman, P., & McElroy, M. B. (2020). Ozone pollution over China and India: Seasonality and sources. *Atmos Chem Phys*, *20*(7). https://doi.org/10.5194/acp-20-4399-2020

Gao, Z., & Zhou, X. (2024). A review of the CAMx, CMAQ, WRF-Chem and NAQPMS models: Application, evaluation and uncertainty factors. *Environ Pollut*, *343*, 23183.

Ghazali, N. A., Ramli, N. A., Yahaya, A. S., Md Yusof, N. F., Sansuddin, N., & Al Madhoun, W. A. (2010). Transformation of nitrogen dioxide into ozone and prediction of ozone concentrations using multiple linear regression techniques. *Environ Monit Assess*, *165*(1-4).

https://doi.org/10.1007/s10661-009-0960-3

Guo, Y., Roychoudhury, C., Mirrezaei, M. A., Kumar, R., Sorooshian, A., & Arellano, A. F. (2024). Investigating ground-level ozone pollution in semi-arid and arid regions of Arizona using WRF-Chem v4.4 modeling. Geosci Model Dev, *17*(10), 4331-4353. https://doi.org/10.5194/gmd-17-4331-2024

Hou, X., Zhu, B., Kumar, K. R., de Leeuw, G., Lu, W., Huang, Q., & Zhu, X. (2020). Establishment of conceptual schemas of surface synoptic meteorological situations affecting fine particulate pollution across eastern China in the winter. *J Geophys Res Atmos*, *125*(23). https://doi.org/10.1029/2020JD033153

Hu, J., Ying, Q., Wang, Y., & Zhang, H. (2015). Characterizing multi-pollutant air pollution in China: Comparison of three air quality indices. *Environ Int*, *84*. https://doi.org/10.1016/j.envint.2015.06.014

Hu, T., Lin, Y., Liu, R., Xu, Y., Ouyang, S., Wang, B., Zhang, Y., & Liu, S. C. (2024). What caused large ozone variabilities in three megacity clusters in eastern China during 2015-2020? *Atmos Chem Phys*, *24*(3). https://doi.org/10.5194/acp-24-1607-2024

Ivatt, P. D., Evans, M. J., & Lewis, A. C. (2022). Suppression of surface ozone by an aerosol-inhibited photochemical ozone regime. *Nat Geosci*, *15*(7). https://doi.org/10.1038/s41561-022-00972-9

Jiang, Z., Li, J., Lu, X., Gong, C., Zhang, L., & Liao, H. (2021). Impact of Western Pacific subtropical high on ozone pollution over eastern China. *Atmos Chem Phys*, *21*(4). https://doi.org/10.5194/acp-21-2601-2021

Ma, Y., Cheng, B., Li, H., Feng, F., Zhang, Y., Wang, W., & Qin, P. (2023) Air pollution and its associated health risks before and after COVID-19 in Shaanxi Province, China. *Environ Pollut*, 320. https://doi.org/10.1016/j.envpol.2023.121090

Mlawer, E. J., Taubman, S. J., Brown, P. D., Iacono, M. J., & Clough, S. A. (1997). Radiative transfer for inhomogeneous atmospheres: RRTM, a validated correlated-k model for the longwave. *J Geophys Res Atmos*, *102*(14). https://doi.org/10.1029/97jd0023

Motesaddi, S., Hashempour, Y., & Nowrouz, P. (2017). Characterizing of air pollution in Tehran: Comparison of two air quality indices. *Civ Eng J*, *3*(9). https://doi.org/10.21859/cej-030911

Petrus, M., Popa, C., & Bratu, A. M. (2024). Determination of ozone concentration levels in urban environments using a laser spectroscopy system. *Environments*, *11*(1). https://doi.org/10.3390/environments11010009

Su, J., Jiao, L., & Xu, G. (2025). Intensified exposure to compound extreme heat and ozone pollution in summer across Chinese cities. *Npj Clim Atmos Sci*, *8*(1). https://doi.org/10.1038/s41612-025-00966-5

Qiu Y, Li X, Chai W, Liu Y, Song M, Tian X, Zou Q, Lou W, Zhang W, Li J, Zhang Y (2025) Insights into ozone pollution control in urban areas by decoupling meteorological factors based on machine learning. Atmos Chem Phys 25(3):1749–63. https://doi.org/10.5194/acp-25-1749-2025

Yang J, Liu J, Han S, Yao Q, Cai Z (2019) Study of the meteorological influence on ozone in urban areas and their use in assessing ozone trends in all seasons from 2009 to 2015 in Tianjin, China. Meteorol Atmos Phys 131(6). https://doi.org/10.1007/s00703-019-00664-x

Jerrett M, Burnett RT, Pope CA, Ito K, Thurston G, Krewski D, Shi Y, Calle E, Thun M (2009) Long-term ozone exposure and mortality. N Engl J Med 360(11). https://doi.org/10.1056/nejmoa0803894

Li M, Liu H, Geng G, Hong C, Liu F, Song Y, Tong D, Zheng B, Cui H, Man H, Zhang Q, He K (2017) Anthropogenic emission inventories in China: A review. Nat Sci Rev 4(6):834–866.

Liao Z, Gao M, Zhang J, Sun J, Quan J, Jia X, Pan Y, Fan S (2024) Mixing-layer-height-referenced ozone vertical distribution in the lower troposphere of Chinese megacities: Stratification, classification, and meteorological and photochemical mechanisms. Atmos Chem Phys 24(6):3541–57. https://doi.org/10.5194/acp-24-3541-2024

Powers JG, Klemp JB, Skamarock WC, Davis CA, Dudhia J, Gill DO, Coen JL, Gochis DJ, Ahmadov R, Peckham SE, Grell GA, Michalakes J, Trahan S, Benjamin SG, Alexander CR, Dimego GJ, Wang W, Schwartz CS, Romine GS, Liu Z, Snyder C, Chen F, Barlage MJ, Yu W, Duda MG (2017) The Weather Research and Forecasting model: Overview, system efforts, and future directions. Bull Am Meteorol Soc 98(8). https://doi.org/10.1175/BAMS-D-15-00308.1

She Y, Li J, Lyu X, Guo H, Qin M, Xie X, Gong K, Ye F, Mao J, Huang L, Hu J (2024) Current status of model predictions of volatile organic compounds and impacts on surface ozone predictions during summer in China. Atmos Chem Phys 24(1). https://doi.org/10.5194/acp-24-219-2024

Sokhi RS, Moussiopoulos N, Baklanov A, Bartzis J, Coll I, Finardi S, Friedrich R, Geels C, Grönholm T, Halenka T, Ketzel M, Maragkidou A, Matthias V, Moldanova J, Ntziachristos L, Schäfer K, Suppan P, Tsegas G, Carmichael G, Franco V, Hanna S, Jalkanen JP, Velders GJM, Kukkonen J (2022) Advances in air quality research–current and emerging challenges. Atmos Chem Phys Discuss 2021:1–133

Sun Z, Tan J, Wang F, Li R, Zhang X, Liao J, Wang Y, Huang L, Zhang K, Fu JS, Li L (2024) Regional background ozone estimation for China through data fusion of observation and simulation. Sci Total Environ 912. https://doi.org/10.1016/j.scitotenv.2023.169411

Touhami D, Mofikoya AO, Girling RD, Langford B, Misztal PK, Pfrang C (2024) Atmospheric degradation of ecologically important biogenic volatiles: Investigating the ozonolysis of (E)-β-ocimene, isomers of α and β-farnesene, α-terpinene and 6-methyl-5-hepten-2-one, and their gas-phase products. J Chem Ecol 50(3–4). https://doi.org/10.1007/s10886-023-01467-6

Trainer M, Parrish DD, Buhr MP, Norton RB, Fehsenfeld FC, Anlauf KG, Bottenheim JW, Tang YZ, Wiebe HA, Roberts JM, Tanner RL, Newman L, Bowersox VC, Meagher JF, Olszyna KJ, Rodgers MO, Wang T, Berresheim H, Demerjian KL, Roychowdhury UK (1993) Correlation of ozone with NOy in photochemically aged air. J Geophys Res 98(D2). https://doi.org/10.1029/92JD01910

Wang K, Zhang Y, Yu S, Wong DC, Pleim J, Mathur R, Kelly JT, Bell M (2021) A comparative study of

two-way and offline coupled WRF v3.4 and CMAQ v5.0.2 over the contiguous US: Performance evaluation and impacts of chemistry-meteorology feedbacks on air quality. Geosci Model Dev 14(11). https://doi.org/10.5194/gmd-14-7189-2021

Wang K, Gao C, Wu K, Liu K, Wang H, Dan M, Ji X, Tong Q (2023) ISAT v2.0: An integrated tool for nested-domain configurations and model-ready emission inventories for WRF-AQM. Geosci Model Dev 16(7). https://doi.org/10.5194/gmd-16-1961-2023

Wang N, Huang X, Xu J, Wang T, Tan ZM, Ding A (2022) Typhoon-boosted biogenic emission aggravates cross-regional ozone pollution in China. Sci Adv 8(2). https://doi.org/10.1126/sciadv.abl6166

Wang P, Zhu SQ, Vrekoussis M, Brasseur GP, Wang S, Zhang H (2022) Is atmospheric oxidation capacity better in indicating tropospheric O3 formation? Front Environ Sci Eng 16(5). https://doi.org/10.1007/s11783-022-1544-5

Wang Y, Duan X, Liang T, Wang L, Wang L (2022) Analysis of spatio-temporal distribution characteristics and socioeconomic drivers of urban air quality in China. Chemosphere 291. https://doi.org/10.1016/j.chemosphere.2021.132799

Wu N, Geng G, Xu R, Liu S, Liu X, Shi Q, Zhou Y, Zhao Y, Liu H, Song Y, Zheng J, Zhang Q, He K (2024) Development of a high-resolution integrated emission inventory of air pollutants for China. Earth Syst Sci Data 16(6):2893–2915. https://doi.org/10.5194/essd-16-2893-2024

Yang J, Shao M (2021) Impacts of extreme air pollution meteorology on air quality in China. J Geophys Res Atmos 126(7). https://doi.org/10.1029/2020JD033210

Yang J, Ke H, Gong S, Wang Y, Zhang L, Zhou C, Mo J, You Y (2025) Enhanced forecasting and assessment of urban air quality by an automated machine learning system: The AI-Air. Earth Space Sci 12(1). https://doi.org/10.1029/2024EA003942

Yin Z, Cao B, Wang H (2019) Dominant patterns of summer ozone pollution in Eastern China and associated atmospheric circulations. Atmos Chem Phys 19(22). https://doi.org/10.5194/acp-19-13933-2019

Zhang C, Jiang Z, Liu M, Dong Y, Li J (2023) Relationship between summer time near-surface ozone concentration and planetary boundary layer height in Beijing. Atmos Res 293. https://doi.org/10.1016/j.atmosres.2023.106892

Zhang H, Wang Y, Hu J, Ying Q, Hu XM (2015) Relationships between meteorological parameters and criteria air pollutants in three megacities in China. Environ Res 140. https://doi.org/10.1016/j.envres.2015.04.004

Zhang J, Gao Y, Luo K, Leung LR, Zhang Y, Wang K, Fan J (2018) Impacts of compound extreme weather events on ozone in the present and future. Atmos Chem Phys 18(13):9861–77. https://doi.org/10.5194/acp-18-9861-2018

Zhang Y, Zhang X, Wang L, Zhang Q, Duan F, He K (2016) Application of WRF/Chem over East Asia: Part I. Model evaluation and intercomparison with MM5/CMAQ. Atmos Environ 124.

https://doi.org/10.1016/j.atmosenv.2015.07.022

Zhao CX, Wang YQ, Wang YJ, Zhang HL, Zhao BQ (2014) Temporal and spatial distribution of PM2.5 and PM10 pollution status and the correlation of particulate matters and meteorological factors during winter and spring in Beijing. Huanjing Kexue 35(2):418–427.

Zhao H, Zheng Y, Li T, Wei L, Guan Q (2018) Temporal and spatial variation in, and population exposure to, summertime ground-level ozone in Beijing. Int J Environ Res Public Health 15(4). https://doi.org/10.3390/ijerph15040628

Zhao ZZ, Zhou Z, Russo A, Du H, Xiang J, Zhang J, Zhou C (2021) Impact of meteorological conditions at multiple scales on ozone concentration in the Yangtze River Delta. Environ Sci Pollut Res 28(44). https://doi.org/10.1007/s11356-021-15160-2

Zheng B, Tong D, Li M, Liu F, Hong C, Geng G, Li H, Li X, Peng L, Qi J, Yan L, Zhang Y, Zhao H, Zheng Y, He K, Zhang Q (2018) Trends in China's anthropogenic emissions since 2010 as the consequence of clean air actions. Atmos Chem Phys 18(19). https://doi.org/10.5194/acp-18-14095-2018

Zhong S, Yu Z, Zhu W (2019) Study of the effects of air pollutants on human health based on Baidu indices of disease symptoms and air quality monitoring data in Beijing, China. Int J Environ Res Public Health 16(6). https://doi.org/10.3390/ijerph16061014

Miao L, Liao XN, Wang YC (2016) Diurnal variation of PM2.5 mass concentration in Beijing and influence of meteorological factors based on long-term data. Huanjing Kexue/Environ Sci 37(8). https://doi.org/10.13227/j.hjkx.2016.08.003

Stieb DM, Doiron MS, Blagden P, Burnett RT (2005) Estimating the public health burden attributable to air pollution: An illustration using the development of an alternative air quality index. J Toxicol Environ Health A 68(13–14). https://doi.org/10.1080/15287390590936120